Stem Cell Reports
Report

ISSCR

OPEN ACCESS

Derivation of Human Midbrain-Specific Organoids from Neuroepithelial Stem Cells

Anna S. Monzel,[1,4] Lisa M. Smits,[1,4] Kathrin Hemmer,[1,4] Siham Hachi,[2] Edinson Lucumi Moreno,[2] Thea van Wuellen,[1] Javier Jarazo,[1] Jonas Walter,[1] Inga Brüggemann,[1] Ibrahim Boussaad,[3] Emanuel Berger,[1] Ronan M.T. Fleming,[2] Silvia Bolognin,[1] and Jens C. Schwamborn[1,*]

[1]Developmental and Cellular Biology, Luxembourg Centre for Systems Biomedicine (LCSB), University of Luxembourg, 7, avenue des Hauts-Fourneaux, 4362 Esch-sur-Alzette, Luxembourg
[2]Systems Biochemistry
[3]Clinical & Experimental Neuroscience
Luxembourg Centre for Systems Biomedicine (LCSB), University of Luxembourg, 4362 Esch-sur-Alzette, Luxembourg
[4]Co-first author
*Correspondence: jens.schwamborn@uni.lu
http://dx.doi.org/10.1016/j.stemcr.2017.03.010

SUMMARY

Research on human brain development and neurological diseases is limited by the lack of advanced experimental in vitro models that truly recapitulate the complexity of the human brain. Here, we describe a robust human brain organoid system that is highly specific to the midbrain derived from regionally patterned neuroepithelial stem cells. These human midbrain organoids contain spatially organized groups of dopaminergic neurons, which make them an attractive model for the study of Parkinson's disease. Midbrain organoids are characterized in detail for neuronal, astroglial, and oligodendrocyte differentiation. Furthermore, we show the presence of synaptic connections and electrophysiological activity. The complexity of this model is further highlighted by the myelination of neurites. The present midbrain organoid system has the potential to be used for advanced in vitro disease modeling and therapy development.

INTRODUCTION

With the development of methods to generate induced pluripotent stem cells (iPSCs) from somatic cells (Takahashi and Yamanaka, 2006; Yu et al., 2007), human cells with the potential to generate all body cell types in vitro became available. This advance led to tremendous progress in the development of protocols for the differentiation of iPSCs into various human cell types. In addition, disease-specific human iPSCs and their derived cell types are now widely used for in vitro disease modeling. However, particularly with regard to neuronal diseases, it is of importance to consider that the human brain is an extremely complex, three-dimensional (3D) structure. Consequently, the investigation of its development and modeling of disease processes in traditional, two-dimensional cultures has strong limitations. It has been demonstrated that the presence of a 3D matrix promotes many biologically relevant functions, such as differentiation capability (Baharvand et al., 2006; Greiner et al., 2013; Tanaka et al., 2004; Tian et al., 2008), cellular signaling, and lineage specification (Engler et al., 2006; Greiner et al., 2013; McBeath et al., 2004). In addition, 3D culture systems are more physiological concerning cell-cell and cell-matrix interactions (Lee et al., 2007). These observations have, in recent years, prompted the use of human iPSCs for the generation of 3D in vitro models of complete organs, the so-called organoids.

These organoid technologies have been pioneered for the small intestine (Sato et al., 2009) and later extended also to other organs or parts of organs (Nakano et al., 2012). Recently, protocols for the generation of human brain-like organoids have been developed, including protocols for cerebral (Lancaster et al., 2013), cerebellar (Muguruma et al., 2015), midbrain-like (Jo et al., 2016), and forebrain organoids (Qian et al., 2016). These organoids provide a proof of concept that human iPSCs can indeed differentiate into various cell types and even self-organize with a specific spatial orientation, which recapitulates key features of the human brain. These brain organoids have been used successfully to model a genetic form of microcephaly (Lancaster et al., 2013) as well as Zika virus-induced microcephaly (Qian et al., 2016). Importantly, thus far all brain organoids have been generated directly from iPSCs; however, evidence suggesting that these organoids could also be derived from more fate-restricted neural stem cells is lacking. The utilization of neural stem cells as the starting population has the advantage that already patterned cells might differentiate into the desired structures more efficiently (cheaper, faster cell doublings, ease of handling, and so forth). Furthermore, while the generation of certain brain structures, such as the cerebral cortex or cerebellum, is meanwhile well described, a higher degree of prepatterning seems to be required for the generation of other highly specialized structures. This is particularly true for brain regions severely affected by neurodegenerative disorders, such as Alzheimer's disease (hippocampus) or Parkinson's disease (PD; substantia nigra).

To address these challenges, we used our previously described human neuroepithelial stem cell (NESC) culture system (Reinhardt et al., 2013) and differentiated these NESCs under dynamic conditions into human midbrain-specific organoids.

RESULTS

Generation of Human Midbrain-Specific Organoids

Previously described NESCs (Reinhardt et al., 2013) were used as the starting population for the generation of human midbrain organoids (hMOs). Compared with iPSCs as a starting population, NESCs are already patterned toward midbrain/hindbrain identity. Therefore, an efficient differentiation into hMOs was expected.

Typically, NESCs express the neural progenitor markers SOX1, SOX2, PAX6, and Nestin prior to organoid generation (Figure S1A). Cells were seeded on round-bottomed ultra-low-adhesion 96-well plates, enabling the cells to form 3D colonies. They were cultured in the presence of the GSK3b inhibitor CHIR99021 to stimulate the canonical WNT signaling pathway, and the SHH pathway was activated using purmorphamine (PMA). The 3D NESC colonies were embedded into droplets of Matrigel for structural support, and 2 days later differentiation into hMOs was initiated. We kept the organoids on an orbital shaker rotating at 80 rpm (Figure 1A). All experiments were conducted with four different and independent NESC lines, individually derived from four different and independent human iPSC lines (Table S1).

During the first 12 days of culture, the hMOs rapidly increased in size and reached a mean core size of 1.26 mm (±0.06 mm, n = 4) in diameter after 20 days (Figure 1B). Consistent with the finding that organoids increased in size after starting the differentiation, we observed expression of the cell proliferation marker Ki67 at day 27 (referred to as early-stage hMOs), which significantly decreased upon maturation until day 61 (late-stage hMOs) from 2.32% (±0.7%, n = 4) to 0.13% (±0.08%, n = 4) (Figures 1C, 1E, and 1G). Furthermore, young hMOs expressed the neural progenitor marker SOX2, which also significantly decreased during maturation from 35% (±3%, n = 4, day 27) to 18.4% (±1.7%, n = 4, day 61). Interestingly, the localization of SOX2-positive cells became more regionally restricted by day 61, resembling the formation of a stem cell niche (Figures 1D, 1F, and 1G). Although consistent with previous findings (Lancaster and Knoblich, 2014; Lancaster et al., 2013), we found substantial cell death in the core of the hMOs, which resulted from the lack of nutrient support in the center of the organoid. In general we did not observe high levels of apoptotic cell death, revealed by staining of the marker cleaved caspase-3. The basic level of apoptosis that was detectable did not change during the course of differentiation (Figure S1B). Importantly, we were able to reproduce the generation of hMOs from NESCs, which were previously derived from four independent iPSC lines.

Neuronal Differentiation and Self-Organization of NESC-Derived hMOs

After showing a decrease of proliferation and stem cell identity, we assessed neuronal differentiation. Because we are particularly interested in the future utilization of hMOs for in vitro modeling of PD, we also investigated the differentiation of midbrain dopaminergic neurons (mDNs). We were able to see robust differentiation into TUJ1-positive neurons and tyrosine hydroxylase (TH) positive mDNs. These stainings revealed the formation of a complex neuronal network (Figures 2A, 2B, S2A, and S2B).

We further examined whether the organoids undergo differentiation into mDNs with midbrain identity. We observed a large population of TH-, LMX1A-, and FOXA2-positive neurons in late-stage hMOs (Figure 2C). Flow-cytometry analysis of late-stage hMOs revealed that 64% (±2.4%, n = 4) of the cells were triple-positive for TH, LMX1A, and FOXA2 (Figure 2D). To further confirm the regional identity of the hMOs, we stained for the orphan nuclear receptor NURR1, which is widely expressed in mDNs. NURR1 expression was observed in early- and late-stage hMOs. We identified cells that co-expressed NURR1 with the midbrain-specific transcription factor OTX2 (Figure 2E) and the mDN marker TH (Figure S2C). We further found cells that co-expressed NURR1 with the ventral marker NKX6-1 (Figures 2F and S2D). We next examined the expression of PITX3, an important transcription factor for the differentiation and maintenance of mDN during development. We found cells co-expressing PITX3 with TH in the late-stage hMOs (Figure S2E) as well as a small population of cells co-expressing PITX3 with NKX6-1 (Figure S2F). Taken together, these results indicate a differentiation toward ventral midbrain identity in the hMOs described here.

To further address the identity of mDNs in these organoids, we stained for the dopamine transporter (DAT), which is a defining marker for mDNs. In late-stage hMOs we identified cells co-expressing TH and DAT (Figure 1G), as well as cells positive for FOXA2/DAT (Figure S2G) and TH/dopamine decarboxylase (DDC) (Figure S2H). qRT-PCR further confirmed the upregulation of the three mDN differentiation markers *TH*, *DAT*, and *DDC* in late-stage hMOs (Figure 2H). Previously, expression of PAX6 in the midbrain but not in mDNs has been shown (Duan et al., 2013; Schwarz et al., 1999). To further confirm the identity of the mDNs, we stained for PAX6 and TH. We could not identify TH-positive mDNs co-expressing PAX6, further

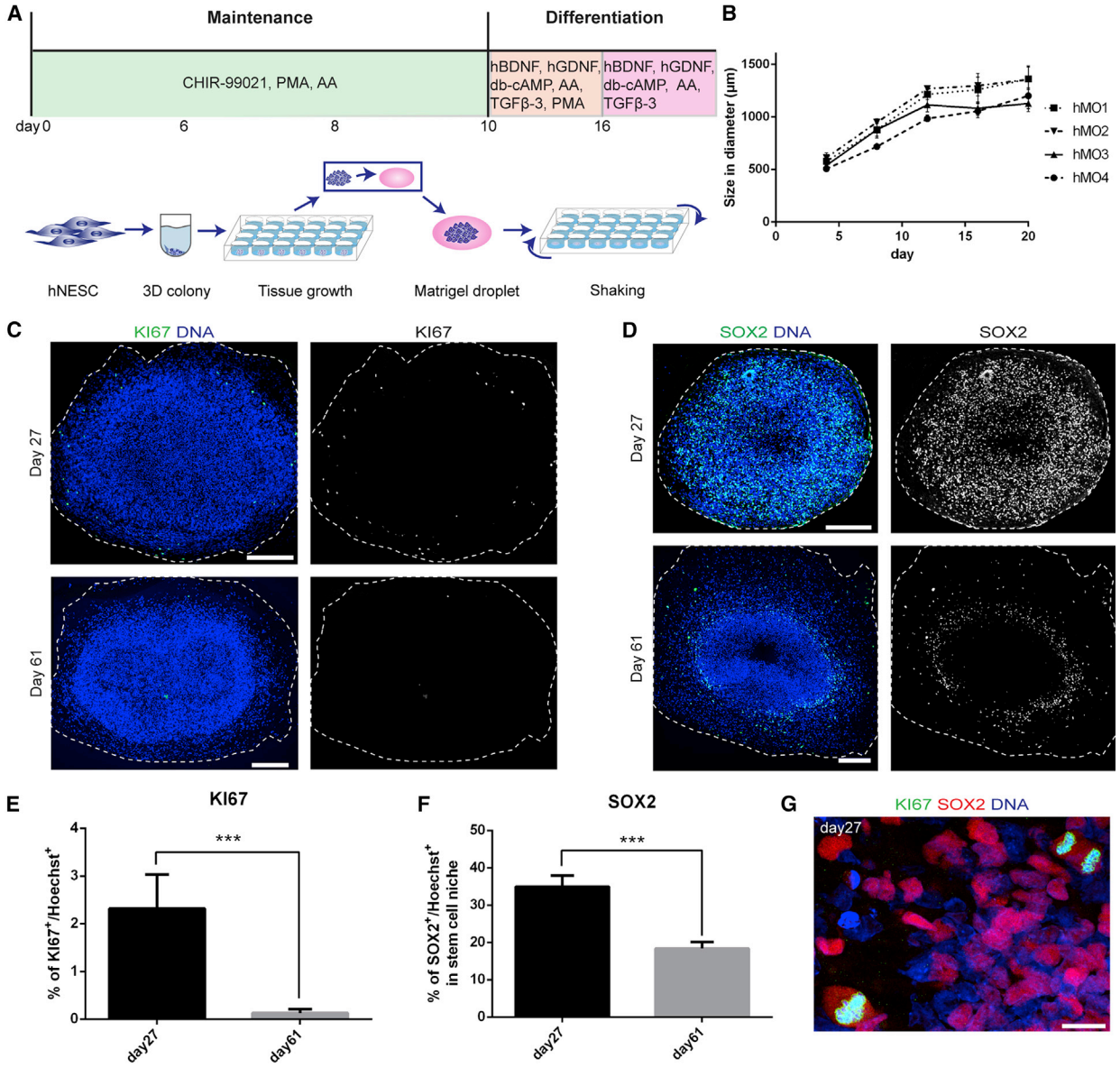

Figure 1. Derivation of hMOs from Human NESCs

(A) Procedure of hMO culture system. Details are described Supplemental Experimental Procedures. hNESC, human neuroepithelial stem cell; AA, ascorbic acid, PMA, purmorphamine.

(B) Growth of hMOs from day 4 to day 20. The diameter size of six organoids (two independent cultures) per organoid line was measured on days 4, 8, 12, 16, and 20 of the organoid culture and the mean was calculated. Error bars represent mean ± SEM.

(C) IF staining of the cell proliferation marker Ki67 at day 27 and day 61 of the organoid culture.

(D) IF staining at day 27 and day 61 of the neural stem cell marker SOX2.

(E) Quantification of the percentage of $Ki67^+$ cells at day 27 and day 61 by cell counting. $Ki67^+$ cells were normalized to $Hoechst^+$ cells. A total of 3,549 $Hoechst^+$ cells (day 27) and 3,309 $Hoechst^+$ cells (day 61) of eight independent organoid cultures derived from four independent lines was counted. Error bars represent mean + SEM (n = 4); ***p < 0.0001.

(F) Quantification of the percentage of $SOX2^+$ cells at day 27 and day 61 by cell counting. $SOX2^+$ cells were normalized to $Hoechst^+$ cells. A total of 3,549 $Hoechst^+$ cells (day 27) and 3,309 $Hoechst^+$ cells (day 61) of eight independent organoid cultures derived from four independent lines was counted. Error bars represent mean + SEM (n = 4); ***p < 0.0001.

(G) Representative image of $Ki67^+/SOX2^+$ proliferative neural progenitor cells at day 27.

Dashed lines indicate the perimeter of the organoid.

Scale bars, 200 μm (C and D) and 20 μm (G).

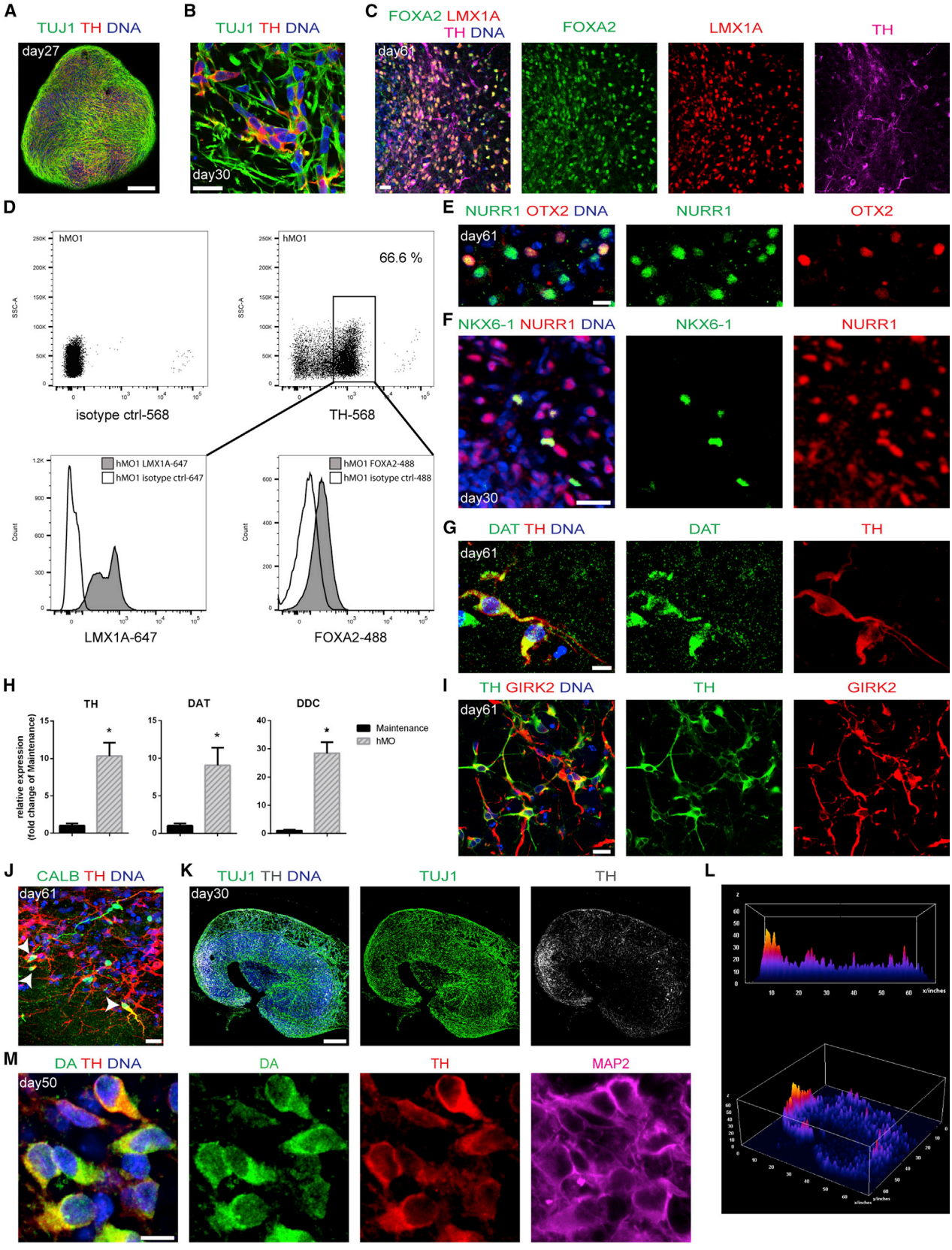

(legend on next page)

supporting that the hMOs contain authentic mDNs (Figure S2I). Intriguingly, we observed robust co-expression of GIRK2 with TH in late-stage hMOs, revealing the presence of the A9 subtype mDNs (Figure 2I), but we also observed cells double-positive for CALBINDIN (CALB) and TH in late-stage hMOs, indicating the presence of A10 subtype mDNs (Figure 2J). These data confirm that our hMOs contain A9 and A10 subtype mDNs.

In previous studies it has been repeatedly shown that stem cells exhibit an enormous potential to self-organize into complex heterogeneous brain organoids (Eiraku and Sasai, 2012; Eiraku et al., 2008; Lancaster et al., 2013; Muguruma et al., 2015). To examine the degree of spatial organization in hMOs, we evaluated the distribution pattern of the mDN markers TUJ1/TH and depicted the results using surface plots. Strikingly, we found that mDNs formed clearly specified clusters within hMOs (Figures 2K and 2L). To further demonstrate the identity of TH-positive neurons as dopaminergic, we analyzed their ability to produce the neurotransmitter dopamine. Immunostaining of mature hMOs demonstrated the presence of dopamine, TH, and MAP2 triple-positive cells (Figure 2M). Intriguingly, we occasionally even observed the formation of Fontana-Masson staining-positive neuromelanin granules in the hMO cultures (Figure S2J).

Altogether these results indicate that mDNs of NESC-derived organoids self-organize into a complex, spatially patterned neuronal tissue.

Glial Differentiation in hMOs

During the development of the fetal human brain, neural tube-derived cells not only differentiate into neurons but also into glia cells, including astrocytes and oligodendrocytes. Therefore, we investigated the presence of these glia cells in the hMOs. In good agreement with brain development, where glia differentiation temporally follows neuronal differentiation, we were unable to detect significant amounts of glia cells in young hMOs (day 27). However, in more mature organoids (day 61), we observed a significant increase of S100B-positive astrocytes (up to 4%) (Figure 3A). We confirmed astrocyte identity by co-staining of S100B with the astrocyte markers Aquaporin (AQP4) and Vimentin (VIM) (Figure 3B). Moreover, we detected a fraction of cells that differentiated into O4-positive oligodendrocytes (Figure S3A). In the CNS, mature oligodendrocytes form myelin sheaths that enwrap axons to accelerate the transmission of action potentials along axons. To analyze whether the oligodendrocytes within the hMOs are able to execute their actual function, i.e., formation of myelin sheets, we performed IF staining against CNPase, a myelin-associated enzyme, together with the neuronal marker TUJ1. A 3D surface reconstruction of these stainings revealed numerous TUJ1-positive neurites that were ensheathed by myelin sheets of CNPase-positive oligodendrocytes (Figures 3C, S3B, and S3C). Interestingly, these neurites often showed gaps of ensheathment, resembling the formation of nodes of Ranvier (Figure 3C) that allow for saltatory fast neuronal transmission. Moreover, CNPase-positive oligodendrocytes that ensheath TUJ1-positive neurites were also positive for the mature oligodendrocyte marker myelin basic protein (MBP) (Figure 3D). Quantification revealed that 29.6% (±2.4%, n = 4) of TUJ1-positive neurites were ensheathed by oligodendrocytes as confirmed by image analysis using MBP and TUJ1 masks.

Functionality of hMOs

One important requirement for neuronal transmission is the development of a mature neuronal network via the formation of synaptic connections. Therefore, synaptic

Figure 2. Neuronal Differentiation and Self-Organization in hMOs

(A) Whole-mount IF staining of an organoid at day 27 for the mDN markers TUJ1 and TH.

(B) IF staining of the mDN markers TUJ1 and TH in a 50-μm section at day 30.

(C) IF staining of the midbrain dopaminergic neuron markers FOXA2, LMX1A, and TH at day 61.

(D) Representative flow-cytometry analysis of cells dissociated from hMO1 at day 61 (six organoids) to quantify TH-, LMX1A-, and FOXA2-positive cells.

(E) IF staining of NURR1 and midbrain marker OTX2 in late-stage hMOs (D61).

(F) IF staining of NKX6-1 and NURR1 in early-stage hMOs (day 30).

(G) IF staining of DAT co-stained with TH in late-stage hMOs (day 61).

(H) qRT-PCR analysis for the mDN markers *TH*, *DAT*, and *DDC*. Data obtained from four independent NESC lines and therefrom derived hMOs. For each hMO culture, five organoids were pooled for RNA isolation. Error bars indicate mean + SEM (n = 4); *p = 0.0286 (TH), *p = 0.0286 (DAT), *p = 0.0571 (DDC).

(I) IF staining of A9 mDN marker GIRK2 co-stained with TH in late-stage hMOs (day 61).

(J) IF staining of A10 mDN marker calbindin and TH in late-stage hMOs (day 61). Arrowheads show cells that are positive for both markers.

(K and L) Asymmetry analysis of mDNs. Immunostaining of mDNs for TUJ1 and TH (K) was analyzed based on fluorescence intensities using a 3D surface plot (L).

(M) IF staining for dopamine (DA), MAP2, and TH at day 50.

Section in (F) is 100 μm and section in (K) is 150 μm. Scale bars, 200 μm (A and K), 20 μm (B, C, F, I, and J), and 10 μm (E, G, and M).

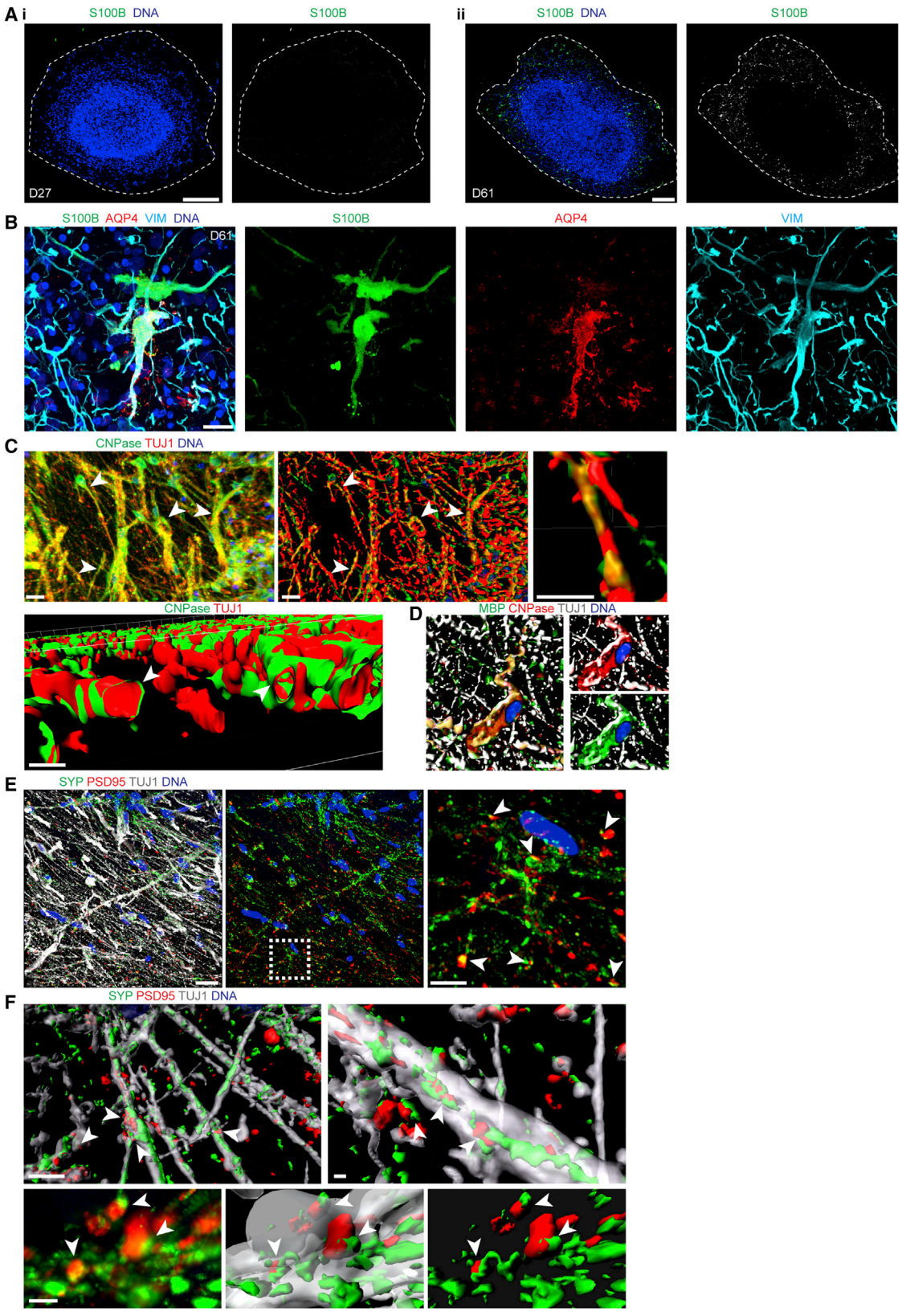

(legend on next page)

connectivity was investigated using IF staining against the presynaptic marker Synaptophysin (SYP) and the postsynaptic marker PSD95 at day 61. To assess the presynaptic and postsynaptic density in hMOs, we quantified the number of presynaptic and postsynaptic counts per μm^2 to an amount of 0.031 (±0.003; n = 4) and 0.016 (±0.004; n = 4), respectively. A subsequent 3D surface reconstruction demonstrated not only the formation of numerous pre- and postsynaptic puncta but also multiple synaptic connections (Figures 3E and S3D). Synaptic connections have been developed between different neurites, indicated by the direct contact of SYP-positive presynapses with PSD95-positive postsynapses (Figure 3F). Accordingly, hMOs fulfill the prerequisite to forward signals via synaptic connections and thus for being electrophysiologically functional.

To further address functionality and neuronal network activity, we performed Fluo-4AM calcium imaging on whole organoids. We measured the spontaneous neuronal activity of six hMOs based on calcium transients evoked by action potentials (Figures 4A, 4B, and S4; Movie S1). Notably, some of the fluorescent traces showed regular firing patterns, which were indicative of tonic electrophysiological activity and resembled the pacemaker activity of mDNs (Hartfield et al., 2014; Moreno et al., 2015). We quantified that 64% (±18%, n = 3) of the cells were actively firing. In addition to calcium imaging, a multielectrode array (MEA) system was used to examine the electrophysiological activity. This methodology allows non-invasive recordings of extracellular field potentials generated by action potentials. At days 82–84, the hMOs were placed on a grid of 16 electrodes in a 48-well tissue culture plate (Figure 4C). Spontaneous activity was detected over several days by individual electrodes in the form of mono- and biphasic spikes (96.13 ± 66.8 spikes/active electrode/measurement [n ≥ 4], Figures 4D and 4E). Furthermore, spikes occurred close in time on multiple electrodes, which represents neuronal network synchronicity (Figure 4F). To further address functionality, we treated the hMOs with the dopamine D_2/D_3 receptor agonist quinpirole (5 μM). Indeed, after this treatment neuronal activity was reduced (Figure 4G), confirming the presence of functional dopamine receptors in the described hMOs. Together, these findings indicate that hMOs develop functional synaptic connections and show spontaneous neuronal activity.

DISCUSSION

One of the main limitations in neuroscience and the modeling of neurological diseases is the lack of advanced experimental in vitro models that truly recapitulate the complexity of the human brain. Here we have presented a human brain organoid system that is highly specific to the midbrain. These hMOs contain spatially patterned groups of dopaminergic neurons, which make them an attractive model for the study of PD. hMOs are characterized in detail with regard to neuronal differentiation and activity as well as for astroglia and oligodendrocyte differentiation.

The presence of astrocytes is crucial for the formation of synapses and regular neuronal activity (Chung et al., 2015). Astrocytes are specified later than neurons during development (Chaboub and Deneen, 2013; Molofsky et al., 2012). Accordingly, hMOs show robust astrocyte immunoreactivity only after 61 days of differentiation. Furthermore, synaptic connections, consisting of a direct contact between pre- and postsynapses, are detectable in the hMOs. These synaptic contacts are the prerequisite for electrophysiological and neuronal network functionality, which we indeed detected in the hMOs by Ca^{2+} imaging and MEA measurements. In addition, fast information transmission between neurons depends on axonal myelination, which is achieved by oligodendrocytes. In most

Figure 3. Differentiation into Glial Cells and Formation of Synaptic Connections

(A) IF staining for the astroglia marker S100B in early-stage (day 27) and late-stage (day 61) hMOs. Dashed lines indicate the perimeter of the organoid.

(B) IF staining for the astrocyte markers S100B, AQP4, and VIM. Dashed lines indicate the perimeter of the organoid.

(C) IF staining of an organoid at day 61 revealing differentiation into CNPase- and MBP-positive oligodendrocytes. 3D surface reconstructions of confocal z stacks visualize the formation of myelin sheaths that enwrap TUJ1-positive neurites (arrowheads) as well as the formation of nodes of Ranvier that are suggested by the presence of gaps of CNPase-positive ensheathment.

(D) 3D surface reconstruction of a confocal z stack of an IF staining of co-stained MBP and CNPase enwrapping a TUJ1-positive neurite.

(E) IF staining of the presynaptic marker SYP and the postsynaptic marker PSD95 at day 61. Arrowheads indicate a direct contact between a pre- and a postsynapse. Dashed box indicates the region of magnification. Images show the 3D view of a confocal z stack.

(F) 3D surface reconstructions of confocal z stacks demonstrate the formation of synaptic connections between different neurites of an organoid as indicated by several direct contacts (arrowheads) between the pre- and postsynaptic markers SYP and PSD95, respectively. Lower panels show high magnifications of a 3D view of a confocal z stack and the corresponding 3D surface reconstruction of several synaptic connections.

Scale bars represent 200 μm (A), 20 μm (B, C upper panel left/middle, E left), 10 μm (C lower panel, D, F upper panel left), 7 μm (E right), 3 μm (F upper panel right), 2 μm (F lower panel), 1 μm C upper panel right.

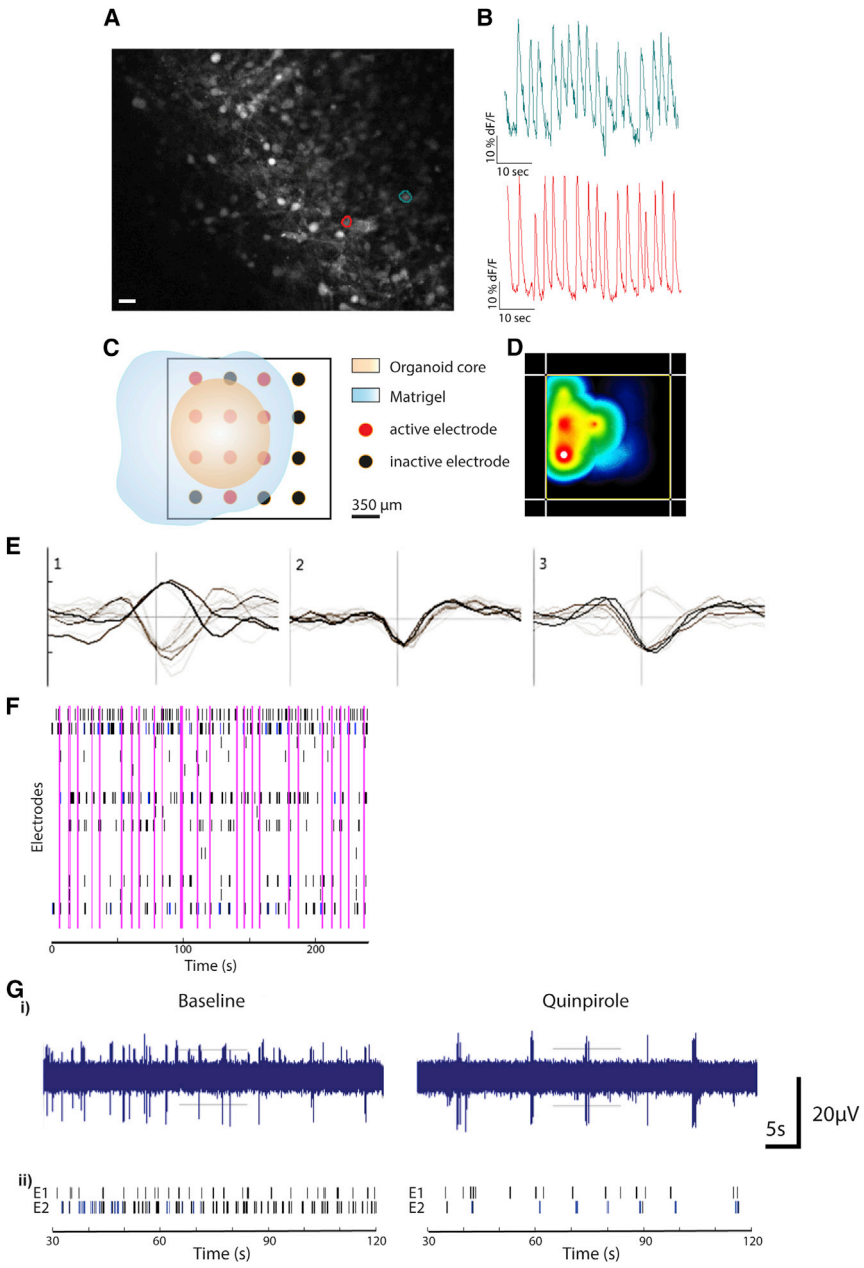

Figure 4. hMOs Reveal Electrophysiological Activity

(A and B) Monitoring of the spontaneous electrophysiological activity in an organoid using Fluo-4AM-based calcium imaging. (A) Mean fluorescence frame of a calcium imaging dataset of a midbrain organoid with two segmented neurons (bordered red and blue) expressing spontaneous activity. Scale bar, 20 µm. (B) Fluorescence traces corresponding to the segmented cell bodies in (A) showing firing patterns with pacemaking-like shape.

(C–F) Evaluation of the spontaneous activity in 16 hMOs of four organoid lines (n = 4) after 82–84 days using an MEA system. (C) Representative scheme of positioned midbrain organoid on a 16-electrode array in a 48-well tissue culture plate. (D) Representative image of the activity map. (E) Examples of mono- and biphasic spikes detected by individual electrodes. (F) Representative image of a spike raster plot showing neuronal network activity in time and space. Spikes occurring on multiple electrodes, closely in time, represent network synchrony, indicated by pink lines. (G) Representative raw data trace (i) and spike raster plots (ii) for single electrodes and the effect of quinpirole on firing frequency of mDNs 30 min after treatment.

stem cell-based differentiation protocols, the differentiation into oligodendrocytes is extremely inefficient (Bunk et al., 2016; Jablonska et al., 2010). However, in the present approach we achieved a robust differentiation into oligodendrocytes and a high degree of neurite myelination. Neurites in these hMOs are ensheathed by oligodendrocytes and even structures such as the nodes of Ranvier, which are of critical importance for saltatory transmission of signals in axons (Faivre-Sarrailh and Devaux, 2013), become apparent.

Compared with other pioneering human brain organoid systems, we are able to generate organoids of a remarkable size (up to 2 mm in diameter) with high reproducibility. Importantly, it was possible to reproducibly generate hMOs based on iPSC lines that come from different origins such as cord blood and fibroblasts. Additionally these fibroblasts have been sampled from individuals at ages from 53 years to 81 years (Table S1). Importantly, in contrast to all other human brain organoid systems, our starting population of cells are not iPSCs but NESCs (Reinhardt et al., 2013), which allows us to achieve an efficient directed differentiation. Our approach is fully focused on the midbrain, as shown by the abundant presence of neurons with mDN identity. These neurons are asymmetrically

distributed in a discrete cluster. This asymmetry mirrors a unique feature of the human brain, where the soma of mDNs reside in the substantia nigra. Furthermore, the presence of neuromelanin, which is a unique feature of the primate brain, is an interesting finding.

The presented hMOs have a great potential to be used for in vitro modeling of diseases that strongly affect the human midbrain, particularly PD (Michel et al., 2016). Patient-specific hMOs might reveal specific phenotypes that are not abundant in 2D cultures and therefore may be used for mechanistic studies and drug testing. Importantly, such a pipeline would be fully suitable for approaches in personalized medicine (Bu et al., 2016; Hillje and Schwamborn, 2016).

Neurodegenerative disorders, such as PD, are typically considered to be age-associated diseases (Sepe et al., 2016; Xu et al., 2016). However, there is accumulating evidence that PD has a strong neurodevelopmental component that probably defines the susceptibility to develop the disease (Garcia-Reitboeck et al., 2013; Le Grand et al., 2014). This finding supports the importance of human brain development models to investigate the disease's underlying mechanisms.

Major limitations of the hMOs presented here, as well as other published brain organoid systems, is the absence of immune cells (microglia) and vasculature. The absence of vasculature might limit the growth of organoids beyond a certain size and the appearance of dead cells in the center of the organoids. While the absence of microglia is a major disadvantage for disease modeling, another option to reduce the problem of the dead cells in the center of organoids might be to produce smaller organoids. However, it seems likely that there is a minimal size of an organoid required to achieve key characteristics such as spatial asymmetry. Despite these limitations, the hMO system presented here along with other models may be a first step toward a more human patient-specific, probably even personalized, era of advanced disease modeling and therapy development.

EXPERIMENTAL PROCEDURES

Authorization from the National Ethics Committee for the work with human iPSCs (CNER No. 201305/04; PDiPS from the Ethic Review Panel of the University of Luxembourg) is in place.

For hMO generation, 9,000 human NESCs were plated in each well of an ultra-low-attachment 96-well round-bottomed plate (Corning) and cultured in N2B27 medium (DMEM-F12 [Invitrogen]/Neurobasal [Invitrogen] 50:50 with 1:200 N2 supplement [Invitrogen], 1:100 B27 supplement lacking vitamin A [Invitrogen], 1% L-glutamine and 1% penicillin-streptomycin [Invitrogen]) containing 3 μM CHIR-99021 (Axon Medchem), 0.75 μM purmorphamine (Enzo Life Science), and 150 μM ascorbic acid (Sigma) (referred to as N2B27 maintenance medium). After 6 days, the colonies were transferred to ultra-low-attachment 24-well plates (Corning) and cultured in N2B27 maintenance medium. On day 8, the 3D colonies were transferred to droplets of hESC-qualified Matrigel (BD Bioscience) as previously described (Lancaster and Knoblich, 2014). Droplets were cultured in N2B27 maintenance medium for 2 more days. On day 10, differentiation was initiated with N2B27 medium supplemented with 10 ng/mL human brain-derived neurotrophic factor, 10 ng/mL human glial-derived neurotrophic factor, 500 μM dibutyryl cyclic AMP (Peprotech), 200 μM ascorbic acid (Sigma), and 1 ng/mL transforming growth factor β3 (Peprotech). In addition, 1 μM purmorphamine (Enzo Life Science) was added to this medium for an additional 6 days. On day 14 of the organoid culture, the plates were placed on an orbital shaker (IKA), rotating at 80 rpm, in an incubator and the organoids were kept in culture with media changes every second or third day. A detailed description is provided in Supplemental Experimental Procedures.

SUPPLEMENTAL INFORMATION

Supplemental Information includes Supplemental Experimental Procedures, four figures, two tables, and one movie and can be found with this article online at http://dx.doi.org/10.1016/j.stemcr.2017.03.010.

AUTHOR CONTRIBUTIONS

A.S.M., L.M.S., K.H., R.M.T.F., S.B., and J.C.S. designed the study; A.S.M., L.M.S., K.H., S.H., E.L.M., T.v.W., J.J., and J.W. conducted the research; A.S.M., L.M.S., K.H., S.H., E.L.M., I. Brüggemann, I. Boussaad, E.B., S.B., and J.C.S. analyzed the data; A.S.M., L.M.S., K.H., S.H., E.L.M., E.B., R.M.T.F., S.B., and J.C.S. wrote the paper.

ACKNOWLEDGMENTS

This project was supported by the LCSB pluripotent stem cell core facility. The J.C.S. laboratory is supported by the Fonds National de la Recherche (FNR) (CORE, C13/BM/5791363) and by a University Luxembourg Internal Research Project grant (MidNSCs). A.S.M., L.M.S., S.H., and E.L.M. are supported by fellowships from the FNR (AFR, Aides à la Formation-Recherche). This is an EU Joint Program - Neurodegenerative Disease Research (JPND) project (INTER/JPND/14/02; INTER/JPND/15/11092422). Further support comes from the SysMedPD project which has received funding from the European Union's Horizon 2020 research and innovation program under grant agreement No. 668738. Finally, we also thank the private donors who support our work at the Luxembourg Center for Systems Biomedicine.

Received: July 1, 2016
Revised: March 10, 2017
Accepted: March 10, 2017
Published: April 13, 2017

REFERENCES

Baharvand, H., Hashemi, S.M., Kazemi Ashtiani, S., and Farrokhi, A. (2006). Differentiation of human embryonic stem cells into

hepatocytes in 2D and 3D culture systems in vitro. Int. J. Dev. Biol. *50*, 645–652.

Bu, L.L., Yang, K., Xiong, W.X., Liu, F.T., Anderson, B., Wang, Y., and Wang, J. (2016). Toward precision medicine in Parkinson's disease. Ann. Transl. Med. *4*, 26.

Bunk, E.C., Ertaylan, G., Ortega, F., Pavlou, M.A., Gonzalez-Cano, L., Stergiopoulos, A., Safaiyan, S., Vols, S., van Cann, M., Politis, P.K., et al. (2016). Prox1 is required for oligodendrocyte cell identity in adult neural stem cells of the subventricular zone. Stem Cells *34*, 2115–2129.

Chaboub, L.S., and Deneen, B. (2013). Astrocyte form and function in the developing central nervous system. Semin. Pediatr. Neurol. *20*, 230–235.

Chung, W.S., Welsh, C.A., Barres, B.A., and Stevens, B. (2015). Do glia drive synaptic and cognitive impairment in disease? Nat. Neurosci. *18*, 1539–1545.

Duan, D., Fu, Y., Paxinos, G., and Watson, C. (2013). Spatiotemporal expression patterns of Pax6 in the brain of embryonic, newborn, and adult mice. Brain Struct. Funct. *218*, 353–372.

Eiraku, M., and Sasai, Y. (2012). Self-formation of layered neural structures in three-dimensional culture of ES cells. Curr. Opin. Neurobiol. *22*, 768–777.

Eiraku, M., Watanabe, K., Matsuo-Takasaki, M., Kawada, M., Yonemura, S., Matsumura, M., Wataya, T., Nishiyama, A., Muguruma, K., and Sasai, Y. (2008). Self-organized formation of polarized cortical tissues from ESCs and its active manipulation by extrinsic signals. Cell Stem Cell *3*, 519–532.

Engler, A.J., Sen, S., Sweeney, H.L., and Discher, D.E. (2006). Matrix elasticity directs stem cell lineage specification. Cell *126*, 677–689.

Faivre-Sarrailh, C., and Devaux, J.J. (2013). Neuro-glial interactions at the nodes of Ranvier: implication in health and diseases. Front. Cell. Neurosci. *7*, 196.

Garcia-Reitboeck, P., Anichtchik, O., Dalley, J.W., Ninkina, N., Tofaris, G.K., Buchman, V.L., and Spillantini, M.G. (2013). Endogenous alpha-synuclein influences the number of dopaminergic neurons in mouse substantia nigra. Exp. Neurol. *248*, 541–545.

Greiner, J., Kaltschmidt, B., Kaltschmidt, C., and Widera, D. (2013). Going 3D—cell culture approaches for stem cell research and therapy. Curr. Tissue Eng. *2*, 8–19.

Hartfield, E.M., Yamasaki-Mann, M., Ribeiro Fernandes, H.J., Vowles, J., James, W.S., Cowley, S.A., and Wade-Martins, R. (2014). Physiological characterisation of human iPS-derived dopaminergic neurons. PLoS One *9*, e87388.

Hillje, A.L., and Schwamborn, J.C. (2016). Utilization of stem cells to model Parkinson's disease—current state and future challenges. Future Neurol. *11*, 171–186.

Jablonska, B., Aguirre, A., Raymond, M., Szabo, G., Kitabatake, Y., Sailor, K.A., Ming, G.L., Song, H., and Gallo, V. (2010). Chordin-induced lineage plasticity of adult SVZ neuroblasts after demyelination. Nat. Neurosci. *13*, 541–550.

Jo, J., Xiao, Y., Sun, A.X., Cukuroglu, E., Tran, H.D., Goke, J., Tan, Z.Y., Saw, T.Y., Tan, C.P., Lokman, H., et al. (2016). Midbrain-like organoids from human pluripotent stem cells contain functional dopaminergic and neuromelanin-producing neurons. Cell Stem Cell *19*, 248–257.

Lancaster, M.A., and Knoblich, J.A. (2014). Generation of cerebral organoids from human pluripotent stem cells. Nat. Protoc. *9*, 2329–2340.

Lancaster, M.A., Renner, M., Martin, C.A., Wenzel, D., Bicknell, L.S., Hurles, M.E., Homfray, T., Penninger, J.M., Jackson, A.P., and Knoblich, J.A. (2013). Cerebral organoids model human brain development and microcephaly. Nature *501*, 373–379.

Le Grand, J.N., Gonzalez-Cano, L., Pavlou, M.A., and Schwamborn, J.C. (2014). Neural stem cells in Parkinson's disease: a role for neurogenesis defects in onset and progression. Cell Mol. Life Sci. *72*, 773–797.

Lee, G.Y., Kenny, P.A., Lee, E.H., and Bissell, M.J. (2007). Three-dimensional culture models of normal and malignant breast epithelial cells. Nat. Methods *4*, 359–365.

McBeath, R., Pirone, D.M., Nelson, C.M., Bhadriraju, K., and Chen, C.S. (2004). Cell shape, cytoskeletal tension, and RhoA regulate stem cell lineage commitment. Dev. Cell *6*, 483–495.

Michel, P.P., Hirsch, E.C., and Hunot, S. (2016). Understanding dopaminergic cell death pathways in Parkinson disease. Neuron *90*, 675–691.

Molofsky, A.V., Krencik, R., Ullian, E.M., Tsai, H.H., Deneen, B., Richardson, W.D., Barres, B.A., and Rowitch, D.H. (2012). Astrocytes and disease: a neurodevelopmental perspective. Genes Dev. *26*, 891–907.

Moreno, E.L., Hachi, S., Hemmer, K., Trietsch, S.J., Baumuratov, A.S., Hankemeier, T., Vulto, P., Schwamborn, J.C., and Fleming, R.M. (2015). Differentiation of neuroepithelial stem cells into functional dopaminergic neurons in 3D microfluidic cell culture. Lab Chip *15*, 2419–2428.

Muguruma, K., Nishiyama, A., Kawakami, H., Hashimoto, K., and Sasai, Y. (2015). Self-organization of polarized cerebellar tissue in 3D culture of human pluripotent stem cells. Cell Rep. *10*, 537–550.

Nakano, T., Ando, S., Takata, N., Kawada, M., Muguruma, K., Sekiguchi, K., Saito, K., Yonemura, S., Eiraku, M., and Sasai, Y. (2012). Self-formation of optic cups and storable stratified neural retina from human ESCs. Cell Stem Cell *10*, 771–785.

Qian, X., Nguyen, H.N., Song, M.M., Hadiono, C., Ogden, S.C., Hammack, C., Yao, B., Hamersky, G.R., Jacob, F., Zhong, C., et al. (2016). Brain-region-specific organoids using mini-bioreactors for modeling ZIKV exposure. Cell *165*, 1238–1254.

Reinhardt, P., Glatza, M., Hemmer, K., Tsytsyura, Y., Thiel, C.S., Hoing, S., Moritz, S., Parga, J.A., Wagner, L., Bruder, J.M., et al. (2013). Derivation and expansion using only small molecules of human neural progenitors for neurodegenerative disease modeling. PLoS One *8*, e59252.

Sato, T., Vries, R.G., Snippert, H.J., van de Wetering, M., Barker, N., Stange, D.E., van Es, J.H., Abo, A., Kujala, P., Peters, P.J., et al. (2009). Single Lgr5 stem cells build crypt-villus structures in vitro without a mesenchymal niche. Nature *459*, 262–265.

Schwarz, M., Alvarez-Bolado, G., Dressler, G., Urbanek, P., Busslinger, M., and Gruss, P. (1999). Pax2/5 and Pax6 subdivide the early neural tube into three domains. Mech. Dev. *82*, 29–39.

Sepe, S., Milanese, C., Gabriels, S., Derks, K.W., Payan-Gomez, C., van, I.W.F., Rijksen, Y.M., Nigg, A.L., Moreno, S., Cerri, S., et al. (2016). Inefficient DNA repair is an aging-related modifier of Parkinson's disease. Cell Rep. *15*, 1866–1875.

Takahashi, K., and Yamanaka, S. (2006). Induction of pluripotent stem cells from mouse embryonic and adult fibroblast cultures by defined factors. Cell *126*, 663–676.

Tanaka, H., Murphy, C.L., Murphy, C., Kimura, M., Kawai, S., and Polak, J.M. (2004). Chondrogenic differentiation of murine embryonic stem cells: effects of culture conditions and dexamethasone. J. Cell Biochem. *93*, 454–462.

Tian, X.F., Heng, B.C., Ge, Z., Lu, K., Rufaihah, A.J., Fan, V.T., Yeo, J.F., and Cao, T. (2008). Comparison of osteogenesis of human embryonic stem cells within 2D and 3D culture systems. Scand. J. Clin. Lab. Invest. *68*, 58–67.

Xu, Y., Yang, J., and Shang, H. (2016). Meta-analysis of risk factors for Parkinson's disease dementia. Transl. Neurodegener. *5*, 11.

Yu, J., Vodyanik, M.A., Smuga-Otto, K., Antosiewicz-Bourget, J., Frane, J.L., Tian, S., Nie, J., Jonsdottir, G.A., Ruotti, V., Stewart, R., et al. (2007). Induced pluripotent stem cell lines derived from human somatic cells. Science *318*, 1917–1920.